Search for a diffuse neutrino emission from the Milky-Way with the ANTARES experiment.

Théophile Cartraud,[a,*] **Julien Aublin,**[a] **Antonio Marinelli,**[†,f,g,h] **Antoine Kouchner,**[a] **Pedro De La Torre Luque,**[†,b] **Daniele Gaggero,**[†,c] **Dario Grasso**[†,d,e] **and Antonio De Benedittis**[†,g] **on behalf of the ANTARES collaboration and for the KRA$_\gamma$ group**[†]

[a]*Université Paris Cité, CNRS, Astroparticule et Cosmologie, F-75013 Paris, France*

[b]*Stockholm University and the Oskar Klein Centre for Cosmoparticle Physics, Stockholm, Sweden*

[c]*Instituto de Física Corpuscular Universidad de Valencia and CSIC Edificio Institutos de Investigacíon, Paterna, Spain*

[d]*INFN Sezione di Pisa Polo Fibonacci, Pisa, Italy*

[e]*Dipartimento di Fisica Università di Pisa, Polo Fibonacci, Pisa, Pontecorvo*

[f]*Dipartimento di Fisica "Ettore Pancini" Università Degli Studi di Napoli "Federico II" Complesso Univ. Monte S. Angelo, Napoli, Italy*

[g]*INFN—Sezione di Napoli Complesso Univ. Monte S. Angelo, Napoli, Italy*

[h]*INAF Osservatorio Astronomico di Capodimonte, Napoli, Italy*

E-mail: cartraud@apc.in2p3.fr, julien.aublin@apc.in2p3.fr

A search for a Galactic diffuse neutrino emission with the latest ANTARES data set is presented. Several models, like the KRA$_\gamma$ or CRINGE predict the neutrino flux produced from the interaction of cosmic rays with atomic and molecular gas in the Milky-Way. The latest ANTARES data samples (track-like and shower-like events induced by different neutrino interactions) are used to test these models via a maximum likelihood ratio method.

ICRC2023
38th International Cosmic Ray Conference
The Astroparticle Physics Conference

---

[*]Speaker

1. Introduction

The interaction of Galactic cosmic rays (CR) with the interstellar medium (gas and radiation fields) produce a flux of secondary particles which are mostly neutral and charged pions, that subsequently decay into $\gamma-$ray photons for the π^0 or neutrinos for the $\pi^{\pm}$. The diffuse flux of gamma rays coming from the galaxy is now precisely measured from GeV up to TeV energies by the Fermi LAT [1]. If the observed $\gamma-$ray emission is primarily driven by hadronic interactions, it is then anticipated that a corresponding flux of neutrinos of comparable intensity will also be present in the same region of the sky. Several searches for a diffuse Galactic emission have already been performed using neutrino telescopes [2, 3, 4, 5, 6], but without finding a significant signal. However the very recent observation of a neutrino flux coming from the Galactic plane by the IceCube experiment [7] brings a convincing evidence that confirms the existence of this expected emission from 500 GeV up to tens of TeV.

The principle of the aforementioned analyses* is to use a model that predict the neutrino flux coming from the galaxy as a template signal in a likelihood analysis. Models with a different morphology have been tested in [7] but the poor angular resolution ($\sim 15 - 20°$) of the selected shower-like events does not allow for a precise discrimination between the models.

The present study uses the ANTARES data, combining track-like and shower-like events with a good angular resolution to provide a complementary search for a diffuse Galactic emission, using a likelihood method. The data selection is explained in section 2 and the different models that are used are described in section 3. The likelihood method is presented in section 4 and the results are summarized in section 5.

2. ANTARES data set

From February 2007 to February 2022, the ANTARES detector have been continuously taking data until its shutdown, reaching a total live time of 4541 days. The current analysis uses two channels: track-like and shower-like events that correspond to different signal topology in the detector. The selection cuts applied to the track channel have been optimized using Monte Carlo (MC) simulations in order to maximize the probability to obtain a p-value at the 3σ level. The procedure selects 7500 track-like events with a median angular resolution of $\sim 0.4°$, and an estimated atmospheric muon contamination of $\simeq 3\%$.

The selection of shower-like events is identical to the one presented in [6], making use of Neural Network and Boosted Decision Tree classifiers developed for the atmospheric ν_e energy spectrum measurement [8]. The selection procedure has been applied to data up to February 2020, the extension to the full ANTARES data taking period will be added in a future study. The current sample contains 1145 shower-like events with a median angular resolution of $\sim 3°$ and a $\simeq 10\%$ atmospheric muon contamination. Both track-like and shower-like events are used in the following likelihood analysis.
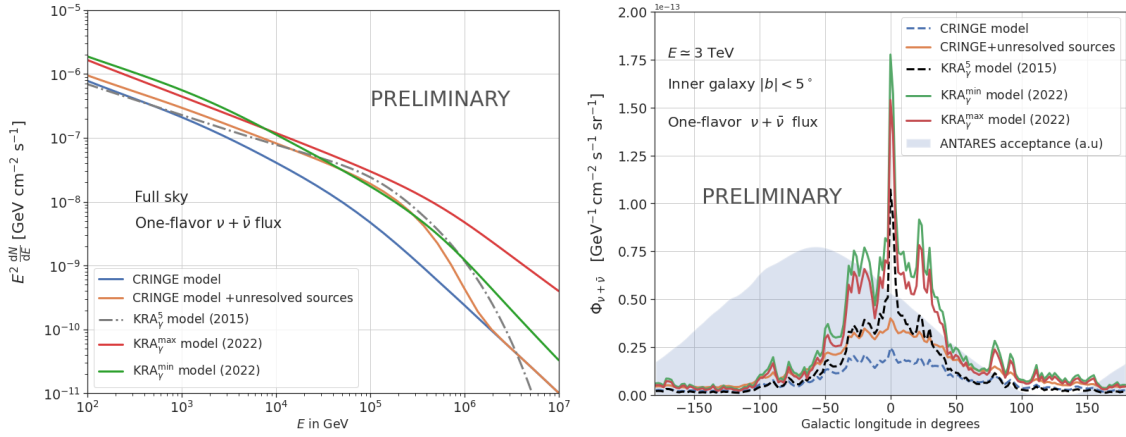
Figure 1: *Left:* Total one-flavor $\nu + \bar{\nu}$ flux integrated over the full sky as a function of energy for the different models. *Right:* average one-flavor $\nu + \bar{\nu}$ flux in the inner Galactic disk ($|b| < 5°$) as a function of the Galactic longitude. The flux is computed for an energy $E \simeq 2.7$ TeV, which depends of the model's convention of binning. The ANTARES acceptance for an $E^{-2.5}$ signal is shown as a blue shaded area.

3. Models of Galactic ν emission

The models that are tested in this study are the so-called KRA_γ models and the CRINGE model. The first version of the KRA_γ [9] provides two different predictions, depending on the value of the assumed energy cut-off in the cosmic ray energy spectrum: at 5 PeV for the KRA_γ^5 or at 50 PeV for the $KRA^{50}\gamma$.

The new version (2022) of the KRA_γ model [10, 11] makes use of more refined and updated cosmic ray and γ-ray measurements, and comes in two configurations: γ-optimized Min and Max that will be called KRA_γ^{min} and KRA_γ^{max} hereafter. These two versions correspond to different assumptions on the CR proton and Helium source spectra, so that the predicted fluxes after propagation bracket the experimental measurement above 10 TeV, which suffer from large uncertainties.

The KRA_γ models use the DRAGON2 code to solve the transport equation of CR distributions, and contrary to the previous KRA_γ^5 model, the neutrino emission prediction is separated for atomic (HII) and molecular (HI) gas clouds. Given a source spectrum, this code provides the propagated spectrum using a non-uniform diffusion coefficient $D(\rho, \vec{x}) \propto \rho^{\delta(\vec{x})}$ as input, which is described by a power law function of the particle rigidity ρ but with a radial dependence of the index $\delta(r/r_\odot)$.

The CRINGE model [12] is mostly based on recent observations of local Galactic cosmic rays from AMS-02, DAMPE, IceTop as well as KASCADE, which have been used to constrain the free parameters of the model. Contrarily to the KRA_γ models, an homogeneous diffusion coefficient $D(\rho)$ is used, with four rigidity breaks and softness parameters as well as five indices δ_i where in particular the last softening $\delta_5 - \delta_4 < 0$ break in the spectrum accounts for the cosmic-ray "knee". Sources of γ rays with fluxes below the experimental detection thresholds, called unresolved sources, have a relative contribution to the diffuse γ-ray flux. In the model these sources are considered to be dominated by pulsar-powered sources. However, whether the associated emission processes are

---

*except for [6] that focuses on the Galatic Ridge region with a counting method

leptonic or hadronic remains undefined, which is why the unresolved sources contribution is either incorporated or not in the CRINGE model.

The π^0 model (2012) [13] used recently in [7] is shown here only for comparison in these proceedings, it will be used in a future update of the present study. The model is based on the π^0 decay into $\gamma-$rays predicted by the GALPROP propagation code, and constrained by Fermi measurements of the $\gamma-$ray flux.

The predictions of all the models are summarized on Figure 1, where the sky-integrated energy spectrum and the longitudinal profile in the Galactic disk are shown. All of these models constitute the templates that are used to build the signal hypothesis in the likelihood, once convoluted with the ANTARES detector response. In practice, the models are available as a collection of Healpix [14] maps, one for each energy bin, except for the π^0 [13] that consists of a unique spatial distribution that should be weighted by a factor $E^{-2.7}$.

4. Description of the analysis

4.1 Likelihood maximization

The analysis uses an unbinned, extended maximum likelihood framework that combines the observations of both track-like and shower-like events. The reconstructed position (α, δ) in equatorial coordinates and reconstructed energy $E^{\dagger}$ of events are the variables used in the likelihood . The Probability Density Functions (PDFs) associated to the signal H_1 and H_0 background hypotheses are written f_s and f_b, and the extended log-likelihood is defined as:

$$\mathcal{L}_{H_1}(\mu_s, \mu_b) \quad = \quad \sum_{i=1}^{n_{\text{tot}}} \log\left[\mu_s\, f_s(\alpha_i, \delta_i, E_i) + \mu_b\, f_b(\alpha_i, \delta_i, E_i)\right] - \mu_s - \mu_b \tag{1}$$

$$\mathcal{L}_{H_0}(\mu_b) \quad = \quad \sum_{i=1}^{n_{\text{tot}}} \log\left[\mu_b\, f_b(\alpha_i, \delta_i, E_i)\right] - \mu_b \tag{2}$$

where the free parameters μ_s and μ_b represent the estimated number of signal and background events in the sample, respectively. As the expected number of signal events are different for the track and shower channels, the signal term is written $\mu_s = r \times \mu_{\text{model}}$ where r is the relative model flux normalization, common to both the track and shower channel, and μ_{model} is the average number of events expected in the considered channel for the base value of the flux, i.e. when $r = 1$.

The generalization to the case of two channels, tracks and showers, is simply

$$\mathcal{L}_{H_1}(r, \mu_b^{(\text{tr})}, \mu_b^{(\text{sh})}) \quad = \mathcal{L}_{H_1}^{(\text{tr})}(r, \mu_b^{(\text{tr})}) + \mathcal{L}_{H_1}^{(\text{sh})}(r, \mu_b^{(\text{sh})}) \tag{3}$$

$$\mathcal{L}_{H_0}(\mu_b^{(\text{tr})}, \mu_b^{(\text{sh})}) \qquad = \mathcal{L}_{H_0}^{(\text{tr})}(\mu_b^{(\text{tr})}) + \mathcal{L}_{H_0}^{(\text{sh})}(\mu_b^{(\text{sh})}) \tag{4}$$

where the likelihood terms for tracks and showers $\mathcal{L}_H^{(\text{tr})}$ and $\mathcal{L}_H^{(\text{sh})}$ are defined by equation 4.1. In this case, there are 3 free parameters, the flux ratio r and the number of background events $\mu_b^{(\text{tr})}$ and $\mu_b^{(\text{sh})}$. This procedure can easily be extended to any number of experimental data sets to combine, provided that all the required PDFs are available.

---

†the letter E is used in the following to designate $\log_{10}(E/1\text{GeV})$

The test statistics is defined as

$$TS = \text{sign}(\hat{r}) \times \left(\max \mathcal{L}_{H_1}(\hat{r}, \hat{\mu}_b) - \max \mathcal{L}_{H_0}(\hat{\mu}_b) \right) \tag{5}$$

where $\hat{r}$ and $\hat{\mu}_b$ are the fitted values that maximize the likelihood. As the free parameters are not bounded, the fitted flux ratio $\hat{r}$ is allowed to be negative, and in that case the test statistic is made negative to keep the meaning of TS as an ordering classification parameter, that should be higher when a positive signal is fitted.

4.2 Probability Density Functions

The Probability Density Functions $f_{s/b}$ represent the probability for an event i of signal/background origin with true variables $\mathbf{x}^{\text{tr}} = (\alpha_i^{\text{tr}}, \delta_i^{\text{tr}}, E_i^{\text{tr}})$ to be detected, selected and reconstructed in the considered channel as $\mathbf{x} = (\alpha_i, \delta_i, E_i)$. In the present analysis, only the position and energy variables are used, but the PDFs are built as a piece-wise function on the energy:

$$f(\alpha, \delta, E) = \begin{cases} f_1(\alpha, \delta) & \text{if } E \in [E_1; E_2[\\ f_2(\alpha, \delta) & \text{if } E \in [E_2; E_3[\\ \vdots \\ f_n(\alpha, \delta) & \text{if } E \in [E_n; E_{n+1}[\end{cases} \tag{6}$$

where $n = 6$ spatial functions are used, each for a given energy bin. This method thus avoids the possible factorization of $f(\alpha, \delta, E) = g(\alpha, \delta) \times h(E)$ which is quite inaccurate for the background, the shape of the function $g(\alpha, \delta)$ being clearly energy-dependent. In practice, the functions $f_i(\alpha, \delta)$ are represented by Healpix maps with a resolution parameter $N\text{side} = 256$ for the track channel, and $N\text{side} = 128$ for the shower channel.

The background PDFs are uniform in right ascension α, thanks to Earth's rotation washing out possible anisotropies in local coordinates after many years of data taking. Thus, each function $f_i(\alpha, \delta)$ in equation 6 is obtained by performing a kernel density estimation (KDE) over the distribution of $\sin \delta$ in real data $f_i(\alpha, \delta) = f_i^{KDE}(\sin \delta)$. If less than 100 events are present in the data, the MC distribution is used instead. The normalization of the functions is then determined by the ratio of the expected number of background MC events in the i-th energy bin to the total number of predicted background events.

The signal PDFs are built by filling a set of initially empty maps with the MC event's reconstructed position and reconstructed energy, with a weight proportional to the value of the model estimated with the true coordinates and energies $\Phi_{\text{model}}(E_i^{\text{tr}}, \alpha_i^{\text{tr}}, \delta_i^{\text{tr}})$. This procedure naturally performs the convolution of the ν flux model with the ANTARES detector's response without the need of any simplified parametrization. To obtain smooth maps even in areas with low statistics, a modified bootstrap method is used to artificially increase the MC statistic, while preserving the properties of the detector's response. The normalization of the functions is similar to the background case, i.e. proportional to the ratio of the signal events in the i-th energy bin to the total number.

Model	KRA_γ^{max}	KRA_γ^{min}	KRA_γ^5	CRINGE + Unresolved	CRINGE
$r_{3\sigma}$	$1.28^{+0.03}_{-0.03}$	$1.47^{+0.03}_{-0.03}$	$1.81^{+0.04}_{-0.04}$	$2.87^{+0.06}_{-0.06}$	$6.67^{+0.16}_{-0.16}$
r_{sens}	$0.63^{+0.18}_{-0.07}$	$0.69^{+0.17}_{-0.09}$	$0.93^{+0.12}_{-0.10}$	$1.47^{+0.18}_{-0.15}$	$3.14^{+0.87}_{-0.47}$

Table 1: Discovery potential at the 3σ level and sensitivity expressed for the fitted flux ratio r, obtained with the combination of track and shower channels.

4.3 Expected performance and optimization

The expected performance of the search can be estimated by simulating MC events with different amounts of injected signal on top of the background. The optimization procedure consists in determining the set of selection cuts that give the lowest possible 3σ discovery potential (DP) flux ratio $r_{3\sigma}$ at 50% level. The number of energy bins n of the PDFs has also been optimized, the best value being $n = 6$ for both track and shower channels. To account for the systematic uncertainty affecting the ANTARES acceptance determination, a Gaussian random fluctuation of 15% in the simulated flux normalization has been applied.

The 3σ discovery potential and the sensitivity (upper limit at 90% CL that would be obtained with the median of the test statistic for the null hypothesis) for the optimized cuts are summarized in Table 1. With the considered models, the probability to obtain a 3σ evidence $p_{3\sigma}$ is always smaller than 50% for the nominal value of the predicted flux, especially for the CRINGE model which would require much more data to be detected by ANTARES. For the γ−optimized max model, which has the best potential, the probability reaches $p_{3\sigma} \simeq 16\%$.

Nevertheless, the sensitivities values suggest that the current analysis has the potential to significantly constrain the KRA_γ family of models, particularly if a very low signal flux is fitted.

5. Results

Model	r^{fit}	μ_s^{fit} (tr/sh)	TS	pre-trial p-value	post-trial p-value	UL90(r)
KRA_γ^{max}	$0.58^{+0.55}_{-0.48}$	9.6/6.7	0.77	$9.80 \cdot 10^{-2}$ (1.65σ)	$1.19 \cdot 10^{-1}$ (1.56σ)	1.35
KRA_γ^{min}	$0.59^{+0.57}_{-0.50}$	9.3/7.2	0.73	$1.06 \cdot 10^{-1}$ (1.62σ)	$1.30 \cdot 10^{-1}$ (1.51σ)	1.45
KRA_γ^5	$0.93^{+0.81}_{-0.70}$	10.2/6.8	0.95	$7.40 \cdot 10^{-2}$ (1.79σ)	$8.92 \cdot 10^{-2}$ (1.70σ)	1.99
CRINGE+Unresolved	$1.08^{+1.18}_{-1.07}$	11.6/8.4	0.50	$1.47 \cdot 10^{-1}$ (1.45σ)	$1.79 \cdot 10^{-1}$ (1.34σ)	2.64
CRINGE	$1.58^{+2.46}_{-1.58}$	8.5/6.8	0.24	$2.35 \cdot 10^{-1}$ (1.19σ)	$2.74 \cdot 10^{-1}$ (1.09σ)	4.57

Table 2: Results of the likelihood analysis: fitted flux r^{fit} with 1σ uncertainty; fitted number of events μ_s^{fit}; test statistics, pre-trial and post-trial p-values of the real data sample, and flux obtained at the sensitivity level for the different models tested. The post-trial p-value for the i-th model is calculated as the fraction of pseudo-experiments (PE) where, for at least one model, the p-value associated with that specific PE is smaller than the pre-trial p-value.

The results of the analysis are summarized on Table 2. None of the statistical tests are significant, the largest excess being found for the KRA_γ^5 with a post-trial p-value equivalent to 1.7σ, with a flux ratio of $r = 0.93$. The best fit flux ratios are around 60% for the KRA_γ^{min} and KRA_γ^{max} models, but with a large uncertainty. For all models, the 90% Neyman confidence intervals have
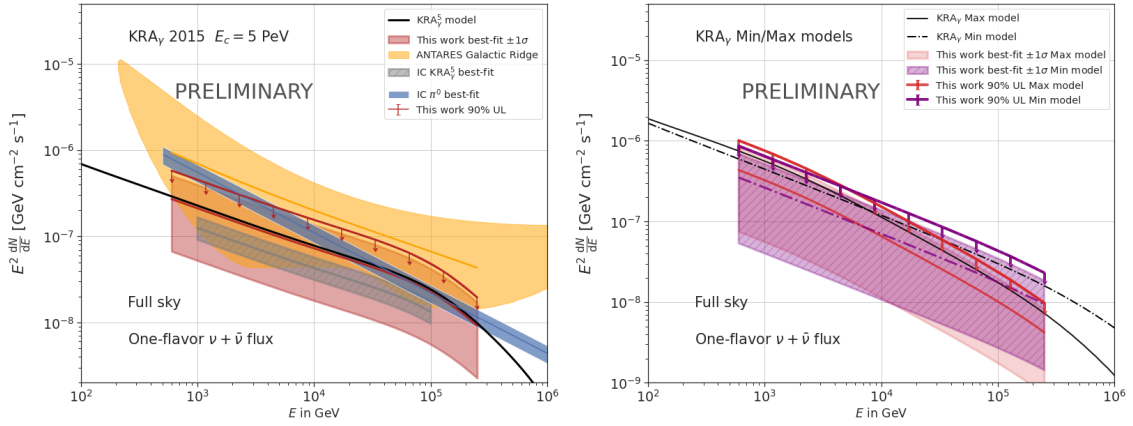
Figure 2: Full sky, one-flavor $\nu + \bar{\nu}$ flux as a function of the energy. *Left:* Results for the KRA_γ^5 model (black line) with a cutoff at $E_c = 5$ PeV (2015) [9]. The present analysis results are plotted in red: the central line with the $\pm 1\sigma$ band shows the best-fit value, and the 90% upper limit is shown with downward arrows. The IceCube best-fit (2023) [7] for the KRA_γ^5 model is shown as a grey band, and the π^0 model best fit as a blue band. The ANTARES Galactic Ridge [6] best fit and 68% contour converted into a full-sky (see text) are shown in orange. *Right:* Results for the KRA_γ^{min} (dashed black line) and KRA_γ^{max} (solid black line) models (2023) [10, 11]. The present analysis result are shown in red and purple, with the same line style as the corresponding models.

been computed and lead to upper-limits, the fitted fluxes being not strong enough to provide a rejection of the zero signal hypothesis at 90%. The upper-limits obtained in this work are listed on the last column of Table 2, and do not constraint any of the considered models.

Figure 2 (left) compares the results obtained in this analysis with the KRA_γ^5 predictions, together with the recent results of IceCube [7]. The best-fit at $\pm 1\sigma$ of the current work is well compatible with the IC result but suffers from a larger uncertainty. The estimation of the flux from the Galactic Ridge with ANTARES data [6] is also shown for comparison. A correction factor has been applied to the contours obtained in [6], as the flux is measured only in the Galactic Ridge Φ_{GR}, defined as the region in Galactic coordinates, $|l| < 30°$, $|b| < 2°$ for track-like events and $|l| < 33°$, $|b| < 5°$ for shower-like events. For a given model, the ratio η_{GR} of the number of track-like and shower-like signal events having their reconstructed coordinates within the Galactic Ridge region divided by the total number of events predicted by the model is computed. For the KRA_γ models, this ratio is found to be energy dependent, and goes from $\eta_{GR}(10\,\text{GeV}) \sim 30\%$ up to $\eta_{GR}(10\,\text{PeV}) \sim 50\%$. For the CRINGE and π^0 models, this ratio is essentially constant and equal to $\sim 20\%$ and $\sim 12\%$ respectively. The best fit value and the 68% contour of the ANTARES Galactic Ridge result has been divided by the function $\eta_{GR}(E)$ computed for the KRA_γ^5 to obtain the plot on Figure 2 (left), where one can see that it is compatible with the IceCube measurements and with the present study. The results for the KRA_γ^{min} and KRA_γ^{max} models are shown in Figure 2 (right).[‡]

[‡]To compare the KRA_γ^{min} and KRA_γ^{max} results with the ANTARES Galactic Ridge results, a similar correction would be applied, using the ratio η_{GR} computed for the KRA_γ^{min} model (the difference in η_{GR} between the two models is less than 2%).

6. Conclusions

The search for a diffuse neutrino emission from the Galaxy with a likelihood method using the latest ANTARES data available has been presented. Several models predicting the neutrino flux with different morphologies and energy distributions have been tested. The higher significance is obtained for KRA_γ^5 with a post-trial p-value equivalent to $1.7\,\sigma$. As none of the statistical tests performed are significant, upper limits on the predicted flux have been set. Those limits do not constraint the models, and the best-fit values obtained by the present analysis are compatible with already published results. The combination of the ANTARES data with other experiments like KM3NeT and IceCube would strengthen even more the evidence for the existence of neutrino flux coming from the Galactic Plane.

References

[1] W. B. Atwood et al. "The Large Area Telescope on the Fermi gamma-ray space telescope mission". In: *The Astrophysical Journal* 697.2 (May 2009), p. 1071.

[2] A. Albert et al. "New constraints on all flavor Galactic diffuse neutrino emission with the ANTARES telescope". In: *Phys. Rev. D* 96 (6 Sept. 2017), p. 062001.

[3] A. Albert et al. "Joint Constraints on Galactic Diffuse Neutrino Emission from the ANTARES and IceCube Neutrino Telescopes". In: *The Astrophysical Journal Letters* 868.2 (Nov. 2018), p. L20.

[4] M. G. Aartsen et al. "Search for Sources of Astrophysical Neutrinos Using Seven Years of IceCube Cascade Events". In: *The Astrophysical Journal* 886.1 (Nov. 2019), p. 12.

[5] M. G. Aartsen et al. "Constraints on Galactic Neutrino Emission with Seven Years of IceCube Data". In: 849.1, 67 (Nov. 2017), p. 67.

[6] A. Albert et al. "Hint for a TeV neutrino emission from the Galactic Ridge with ANTARES". In: *Physics Letters B* 841 (2023), p. 137951.

[7] IceCube Collaboration et al. "Observation of high-energy neutrinos from the Galactic plane". In: *Science* 380.6652 (2023), pp. 1338–1343.

[8] A. Albert et al. "Measurement of the atmospheric ν_e and ν_μ energy spectra with the ANTARES neutrino telescope". In: *Physics Letters B* 816 (2021), p. 136228.

[9] Daniele Gaggero et al. "The gamma-ray and neutrini sky: a consistent picture of Fermi-LAT, MILA-GRO, and IceCube results". In: *The Astrophysical Journal Letters* 815.2 (Dec. 2015), p. L25.

[10] P. De La Torre Luque et al. "Prospects for detection of a galactic diffuse neutrino flux". In: *Frontiers in Astronomy and Space Sciences* 9 (2022).

[11] De La Torre Luque, P. et al. "Galactic diffuse gamma rays meet the PeV frontier". In: *A&A* 672 (2023), A58.

[12] Georg Schwefer, Philipp Mertsch, and Christopher Wiebusch. "Diffuse Emission of Galactic High-energy Neutrinos from a Global Fit of Cosmic Rays". In: *The Astrophysical Journal* 949.1 (May 2023), p. 16.

[13] M. Ackermann et al. "Fermi-LAT observations of the diffuse γ-ray emission: implications for cosmic rays and the interstellar medium". In: *The Astrophysical Journal* 750.1 (Apr. 2012), p. 3.

[14] K. M. Górski et al. "HEALPix: A Framework for High-Resolution Discretization and Fast Analysis of Data Distributed on the Sphere". In: *The Astrophysical Journal* 622.2 (Apr. 2005), p. 759.